ISA Transactions 100 (2020) 46–62

Contents lists available at ScienceDirect

ISA Transactions

journal homepage: www.elsevier.com/locate/isatrans

Research article

Robust control of automatic voltage regulator (AVR) with real structured parametric uncertainties based on H_∞ and μ-analysis

Mohammadreza Modabbernia, Behnam Alizadeh *, Alireza Sahab, Maziar Mirhosseini Moghaddam

Department of Electrical Engineering, Lahijan Branch, Islamic Azad University, Lahijan, Iran

ARTICLE INFO

Article history:
Received 2 August 2018
Received in revised form 24 December 2019
Accepted 3 January 2020
Available online 13 January 2020

Keywords:
AVR
Automatic voltage regulator
Robust control
H infinity
μ-analysis

ABSTRACT

Within this work, a novel controller in terms of *H* infinity (H_∞) and structured singular value decomposition has been presented to provide the robust performance of the Automatic Voltage Regulator (AVR) system Six real structured uncertainties in actuator, exciter and generator have been assumed for the linear transfer functions of the AVR system. Each uncertain parameter varies between a minimum and a maximum value due to the load variations in a period of time and aging effects over the life time. The efficiency of the presented design lies on two main reasons. The first is the simultaneous considering of the output disturbances, sensor noises and system uncertainties in the controller design approach. The second is the non-conservative modeling of all six structured parameters in the required μ-synthesis $P-\Delta-K$ configuration. By suboptimal H_∞ control design technique and μ-analysis theorem, a single input single output (SISO) controller comprising a closed loop system with μ<1 is obtained. The offered controller's supremacy is represented through comparison of its performance with some other optimized PID, PIDD fractional order PID (FOPID), fuzzy + PID and Interval Type-2 fuzzy logic controllers by heuristic optimization algorithms. The simulation outcomes indicate that the provided robust controller for the AVR system has the better performance than the other optimized and fuzzy controllers in a wide range of the uncertainties. Also, the better behavior of the intended robust controller was shown in two benchmarks: a single machine connected to a 230kV network, and a four-machine two-area test system.

1. Introduction

In exciting system of a synchronous generator, the generator terminal voltage is sensed and differed from a reference value and the automatic voltage regulator (AVR) changes the field voltage of the generator based on this error signal for controlling the reactive power flow to the load. On the other hand, the main obligation of an AVR is to set a synchronous generator's terminal voltage magnitude of at a distinguished level [1,2].

Owing to some complex performance of the power system such as nonlinearity of the system characteristics, variation of the load, variable operating points and great inductance of the generator field windings, achieving the fast and stable response of the regulator is challenging [3]. Hence, improving the behavior, robustness and speed of the AVR is important utilizing a controller to ensure the efficient response of the closed loop system to transient alterations in terminal voltage.

As a result of the easy usage and simple structure of the proportional–integral–derivative (PID) controllers in the industry [4], they have been widely used to establish a good performance for the AVR system. In the recent years, by development of the heuristic optimization algorithms, it can be seen that a lot of optimized PI, PID controller and its derivatives like fractional order PID (FOPID) and Fuzzy PID controller have been proposed for the AVR systems based on these optimization algorithms. Designing of a decentralized PI controller and tuning its elements through Bacteria Foraging (BF) and BF-particle swarm optimization (BF-PSO) techniques have been discussed in [5]. The PID controllers have been optimized by particle swarm optimization (PSO) approach [6], artificial bee colony (ABC) algorithm [7], Shuffled Frog Leaping (SFL) Algorithm [8], Simplified Particle Swarm optimization algorithm [9], Taguchi Combined Genetic algorithm method [10], Local Unimodal Sampling Algorithm [11], Imperialistic Competition Algorithm (ICA) [12] and Teaching Learning Based Optimization (TLBO) Algorithm [13,14]. And Shayeghi et al. have proposed a fuzzy logic-based controller which is known as Fuzzy P+FuzzyI+FuzzyD (FP + FI + FD) controller for AVR system and then optimized the controller parameters by hybrid of PSO (HGAPSO) method and Genetic Algorithm (GA) [15]. A fuzzy logic

* Corresponding author.
E-mail addresses: m_modabbernia94@stumail.liau.ac.ir (M. Modabbernia), behnam_alizadeh@liau.ac.ir (B. Alizadeh), sahab@liau.ac.ir (A. Sahab), m.mirhosseini@liau.ac.ir (M.M. Moghaddam).

https://doi.org/10.1016/j.isatra.2020.01.010
0019-0578/

method and combined GA have been presented by Devaraj and Selvabala to calculate the optimal PID controller factors in AVR system [16].

An enhanced evolutionary non-dominated sorting genetic algorithm II (NSGA II) improved with a chaotic map for higher efficiency, has been used for the multi-objective optimization of AVR system in [17] and [18]. A chaotic ant swarm optimization technique was represented by Tang et al. [19]. In [20] and [21] PSO algorithm was carried out for designing the FOPID controller. A direct Fractional Order Model Reference adaptive Controller (direct FOMRAC) has been presented for an AVR, in which the controller parameters have been set through adaptive laws determined by fractional order differential equations [22]. Zhang et al. have proposed an enhanced artificial bee colony algorithm combining cyclic exchange neighborhood with chaos (CNC-ABC), concerning about tuning the parameters of FOPID controller [23]. In [24] the AVR system's different performance criteria have been structured as system norms and then coupled with an evolutionary multi-objective optimization (MOO) algorithm. FOPID controller has been designed using ICA optimization algorithms for an AVR system [25]. Mukherjee and Ghoshal have focused on optimum tuning the PID controller for the AVR utilizing craziness-based PSO (CRPSO) and binary coded GA [26]. The behavior of F-PID, PID, and GA-F-PID controllers for improvement of energy effectiveness of a dynamic energy system has been examined by Jahedi and Ardehali [27]. The discrete fuzzy PID controller has been used to single machine infinite-bus (SMIB) model in [28]. An iterative learning control (ILC) algorithm as a control rule has been used to maintain voltage error of AVR further low in [29]. A PID fractional order controller optimized by cuckoo search based algorithm is introduced in [30]. A fuzzy logic + PID controller optimized by TLBO algorithms is introduced in [31]. An Interval class-2 fuzzy logic controller in terms of interval value sets has been introduced by Panda et al. for modeling the imprecision from the uncertainty of the AVR system [32]. The PSO algorithm has been used to tune the four advances in the PID plus second order derivative controller ($PIDD^2$) by Sahib [33]. Prasad and et al. have presented an adaptive optimal control design method for AVR system utilizing policy iteration system according to adaptive critic outline [34]. In [35], a novel controller has been designed for voltage control and load frequency control (LFC) of a single area power system based on the combination of neural networks and fast traversal filters. The main target of these papers is generally optimization of the controller coefficients around a nominal point of the system. The differences of these researches are mostly in their optimization technique and the robustness of their controllers has not been proven by mathematical approaches.

The robust control and μ-theorem have been dramatically exploited to enhance the performance of power systems in the last two decades [36]. A robust load frequency controller has been intended in terms of μ-synthesis in a not tamper conditions for electric power system in [37]. The μ-synthesis has been used to carry out the robust stability of an interconnected distributed energy resource in [38]. Some robust control strategies have been developed based on μ-theorem for reducing the microgrid frequency deflection in [39,40]. A nonlinear artificial neural network (ANN) controller on the basis of μ-synthesis method has been introduced by Shayeghi and Shayanfar [41].

In [42] a strong multivariable controller was synthesized for exciting system containing the AVR and a supplementary transient stability controller. The parameters are modeled as unstructured uncertainties through plotting the system's frequency responses under different operating circumstances and a bound is selected to provide the greatest uncertainties. Without introducing the equation of the controller, a decentralized H_∞ controller for a multi machine power system has been proposed in [43] for obtaining damping the power system oscillations and terminal voltage control simultaneously.

For power system stabilizing, some strategies have been introduced without considering the structured parameters of the system. In these studies, the effects of the deviation points have been modeled by additive unstructured uncertainties. By this kind of uncertainties, we will act conservative [44]. In other words, the uncertainty modeling in this manner has been done only for some operating points and the intervals of the parameters deviation have not been considered. Also, the equations of the designed controller are not presented in these papers. An H_∞ power system stabilizer (PSS) has been proposed by Chen and Malik [45]. Also, this PSS controller has been suggested by Folly et al. with the 'numerator–denominator' uncertainty representation [46]. By the same token, Chen and Malik have offered a strong controller in terms of μ-theorem respecting the PSS system [47].

According to the above-mentioned points, the introduced references can be classified based on four patterns:

(1) The papers about AVR controller design by (evolutionary) optimization algorithms.
(2) The robust strategies in synchronous generator load frequency control (LFC).
(3) The robust approach of power system stabilizer (PSS).
(4) Robust control of the AVR system.

Separation of the structures of the AVR, LFC and PSS systems [1,48] causes the patterns #2 and #3 (robust control of LFC or PSS) to be different from the matter of this research. They are presented only to show the ability and spread of the robust theorem in power systems. Also, some other usages of the robust control approaches could be seen in new power system applications [49–56]. When authors introduce a PID, Fractional order controller, fuzzy logic controller and so on for AVR system (pattern 1), their target is usually optimization of the controller coefficients around a nominal point. The differences of these researches are mostly in their optimization techniques. So, the robustness has not been mathematically proven and their performance is only shown by the simulation of the closed-loop system around some values of its parameters with some tolerances (e.g. see [9,11,12,14,30,57]). When a robust control strategy is proposed to control the voltage of the synchronous generator (pattern #4), mostly the transfer function (TF) or steady-state equations of the designed controller have not been introduced by the authors [42,43]. Perhaps, it comes from the fact that the order of robust controllers which are obtained from H infinity or mu theorems, are so high, therefore, the authors are reluctant to show the equations of their designed controllers. Also, none of these papers has considered the parameters of the AVR system as structured uncertainties. The synchronous generator models with the deviation ranges of their real parameters are exactly characterized in the literature and textbooks, and their practical outcomes are approved. Therefore, these real structured parametric uncertainties can be used in the robust control approach to avoid conservation [44]. Although, the design and analysis would be even harder regarding the real numbers, [44].

The AVR linear time invariant (LTI) model parameters vary based on the operating points broadly [47]. Accordingly, the robust performance of a controller designed for the nominal point of the AVR system is not guaranteed. So, designing a controller to enhance the AVR system's robust performance was always felt. But, why do we need μ-theorem to control the AVR system? This is an important question.

Designing a controller for the AVR system based on the linear control schemes requires a nominal LTI power system model

obtained from a particular operating condition. This model's parameters of show the power system dynamic behavior around the previously mentioned nominal condition and they have real values that vary between their minimum and maximum amounts. Since these parameters are real structured uncertainties, H_∞ is a proper technique to improve the AVR system's robust performance and μ-theorem is a direct method to analyze its robust performance. Singular value decomposition (μ) theorem has been introduced by J. Doyle in 1982 [58]. It is a strong tool to analyze and design the robust control systems with real structured uncertainties [44,59]. the main targets of using the H infinity and Mu theorems are: considering the system parameters as real parametric uncertainties, limiting the controller's output, and direct modeling of the output disturbances and noise. These targets were noticed based on some crucial ideas as achieving a single input-single output (SISO), minimum phase, and minimum degree linear controller with the robust performance which can be replaced directly with minimum cost instead of the industrial voltage controller without any changes in the AVR system, sensors type and actuators structure. The introduced linear robust controller can be taken into account in studying the performance of some other robust controllers which will be designed by other linear (loop-shaping and quantitative feedback theory) or nonlinear approaches like disturbance observer to compensate for uncertainties [60–62] in the future.

A non-complex AVR system includes 4 main subsystems known as amplifier, generator, sensor, and exciter. In a simple linear transfer function (LTF) form, all of these four blocks can be modeled by a one-order LTF that has a time constant and a gain. By considering the small alterations in the gain and the time constant of the sensor transfer function, it will be taken out of the uncertain set. Hence, the AVR system will have six real structured uncertainties. These uncertainties are the amplifier's time and gain constants, exciter and synchronous generator.

This paper presents a novel single input (the synchronous generator's terminal voltage) single output (field voltage of the synchronous generator) robust controller for the AVR. This controller was designed by H_∞, μ-theorem to achieve the robust performance of the AVR systems in the attendance of six real parametric and structured uncertainties. The greatest benefit of a robust control method is the possibility of considering the modeling of the uncertainties, the system disturbances and the sensor noises at the controller design procedure. The suggested controller's performance was assessed by time domain simulation of three case studies in MATLAB and Simulink. The results of simulating show that the accomplishment of the propounded robust controller for the AVR system is superior to the other optimized PID controllers in terms of the heuristic algorithms and IEEE exciting system. Also, the last case study shows that the designed controller has the better behavior than the additional terminal voltage controller as the PSS without the need to a frequency sensor.

The paper mainly contributes in: (i) Considering the AVR system parameters (time constants and gains of the amplifier, exciter, and generator) as structured real parametric uncertainties without any conservation. (ii) Selecting the good weighting functions for modeling the robust performance of the AVR closed-loop system. (iii) Proposing a general structure for the AVR system based on the system structured uncertainties as P-Δ-K representation which could be used with some other robust controller approaches like D–K iteration, mixed H_2/H_∞, H_∞ loop-shaping and so on. (iv) Designing a single input-single output (SISO) robust controller from order six which could be replaced instead of any industrial AVR PID controller. (v) Introducing a step by step approach to design the robust H_∞ controller for the AVR system of the synchronous generator in a large size power system.

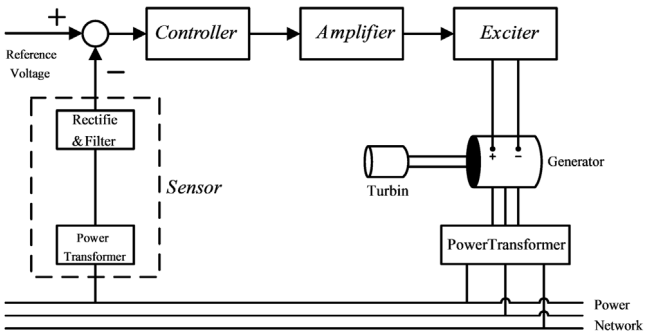

Fig. 1. The schematic diagram of a typical single-machine infinite-bus system.

The remainder of this study was structured as: Section 2 describes the AVR system model and depicts its block diagram and design objectives. An abridged introduction to the μ-theorem and H_∞ method is given in Section 3. In Section 4, the procedure of constructing the P-Δ-K configuration of the AVR system with six real structured uncertainties has been discussed. By selecting some good weighting function and using the H_∞ and μ-analysis techniques, a single input single output (SISO) robust controller has been set forth in Section 5. Section 6 copes with assessing the controller robust performance by means of simulations in MATLAB and providing the comparison of the results with some other heuristic optimized PID, FOPID and fuzzy controllers. In Sections 7 and 8, two benchmark problems of the single machine connected to a 230 kV network and the four-machine two-area test system have been simulated and compared by the designed robust controller and generalized IEEE excitation system, respectively. Finally, the presented method is concluded in Section 9.

2. AVR system's transfer function model

The schematic diagram of a typical SMIB power generation system has been demonstrated in Fig. 1. The system consists of a synchronous generator linked to infinite bus. The electrical system section has two main control loops as AVR and automatic load-frequency control (ALFC) and one supporting controller as PSS to adjust the load frequency and local voltage terminal automatically. The shaft frequency of the generator has been sensed and a governor controls mechanical power and speed of the rotor based on a turbine.

Controlling the excitation voltage of the synchronous generator is a key element to enhance the power system stability and performance. The AVR varies the excitation voltage of the generator to retain its output voltage at a specific level.

In its simple form, the AVR system basic components known as exciter, amplifier, sensor, and generator each can be modeled by a one-order transfer function with a time constant and gain. With the load variations, change of operating points, system parameters aberration and so on, the time constants and gains of the AVR components transfer functions can be varied based on Table 1 ([7,11,16] and [33]). In schematic diagram of Fig. 1, the AVR system has a block diagram with five individual blocks. This block diagram has been shown in Fig. 2.

3. μ-synthesis and P-Δ-K representation

The systems with uncertain dynamics can be reflected in the M-Δ configuration of Fig. 3. The structure of uncertain block is

Table 1
Transfer function of AVR components.

Component	Transfer function	Gain limit	Time constant limit
Amplifier	$G_A = \frac{K_A}{T_A s+1}$	$10 \le K_A \le 40$	$0.02\,\text{s} \le T_A \le 0.1\,\text{s}$
Exciter	$G_E = \frac{K_E}{T_E s+1}$	$1 \le K_E \le 10$	$0.4\,\text{s} \le T_E \le 1\,\text{s}$
Generator	$G_G = \frac{K_G}{T_G s+1}$	$0.7 \le K_G \le 1$	$1\,\text{s} \le T_G \le 2\,\text{s}$
Forward transfer function	$G_F = G_A G_E G_G = \frac{K_F}{(T_A s+1)(T_E s+1)(T_G s+1)}$	$7 \le K_F \le 400$	
Sensor	$G_S = \frac{K_S}{T_S s+1}$	$K_S = 1$	$T_S = 0.006\,\text{s}$

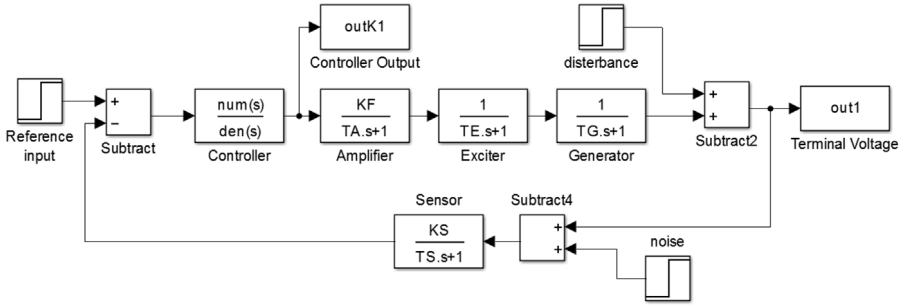

Fig. 2. The block diagram of the AVR system.

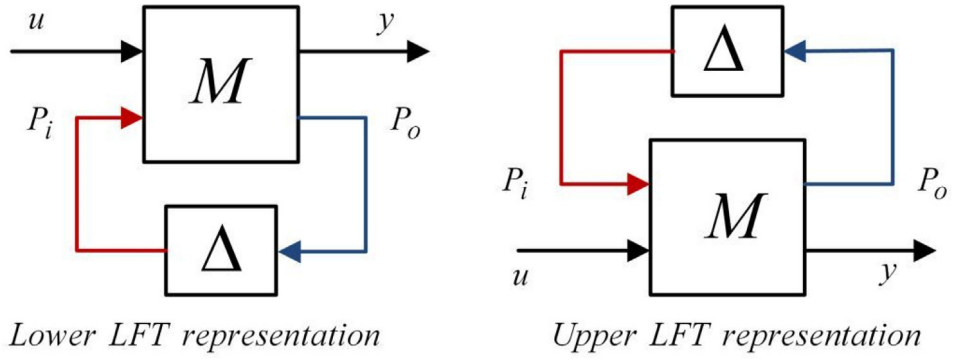

Fig. 3. M-Δ representation of the system.

defined as:

$$\Delta = diag[\delta_1 I_{r1}, \ldots, \delta_s I_{rs}, \Delta_1, \ldots, \Delta_t] \quad \delta_i \in C, \quad \Delta_j \in C^{m_j \times m_j} \tag{1}$$

where $\sum_{i=1}^{s} r_i + \sum_{j=1}^{t} m_j = n$ and n is the dimension of the block Δ. The transfer function matrix M usually includes the controller K and plant P based on a closed-loop interconnected matrix.

$$M(P, K) = F_L(P, K) \tag{2}$$

To analyze and design a controller regarding a model with uncertainties, the representation of Fig. 4 has been proposed instead of Fig. 3. In Fig. 4, u denotes the exogenous inputs of the system such as disturbances, command signals, noise, etc. e depicts the error output typically containing system output, filtered output signals, tracking errors, etc. P_o and P_i represent the output and input signals of the uncertainties, respectively. y reflects the feedback signals that are the inputs of the controller and C indicates the control signals of system which come from the controller. P shows the nominal open-loop interconnected transfer function matrix. It neither contains the controller K nor any uncertainties nor perturbations. The robust stability (RS) and the robust performance(RP) of a system can be written as [44]:

- Robust performance: $(RP) \Leftrightarrow \mu_{\tilde{\Delta}}(M) < 1$ for mixed structured and unstructured uncertainty $\tilde{\Delta}$.
- Robust stability: $(RS) \Leftrightarrow \mu_{\Delta}(M_{11}) < 1$ for structured uncertainty Δ.
- Nominal performance: $(NP) \Leftrightarrow \|M_{22}\|_\infty < 1$.
- Nominal stability: $(NS) \Leftrightarrow M$ is internally stable.

By the unstructured uncertainty Δ, the robust stability requirement equals to $\|M_{11}\|_\infty < 1$. Also, for the robust stability robust performance (RSRP) design, finding a controller K is necessary that:

$$\underset{\omega \in R}{SUP}\, \mu_{\tilde{\Delta}}[M(P, K)(j\omega)] < 1 \tag{3}$$

Consequently, the first step in analyzing or designing a controller on the basis of μ-synthesis is the definition of the P-Δ-K representation of the perturbation system. In this paper, the P-Δ-K structure of the AVR system has been introduced under this assumption that the time constants and gains of the amplifier, the exciter and the synchronous generator are real parametric uncertainties.

4. P-Δ-K representation of AVR system without weighting functions

The unstructured uncertainties have been used to model the dynamic perturbation such as non-modeled or high frequency dynamics of the system [44]. When the linear model of the

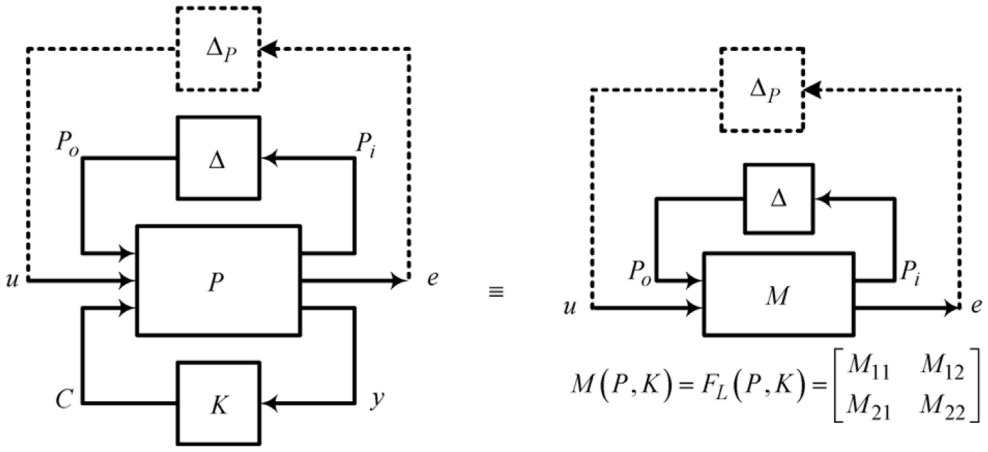

Fig. 4. P-Δ-K representation of robust control system.

system exists and its perturbation is defined based on some parameters containing real values that vary in an interval, the structured or parametric uncertainties will be used to introduce them [44]. When the system uncertainties are real, the robust controller analysis and synthesis would be even harder (page 22 of [44]). In such cases, for example, the AVR system, seemingly, utilizing a whole, full block unstructured uncertainties to define the real parametric uncertainties would direct to a cynical study of plant treatment and conservative operation (page 23 of [44]). In this paper and other papers about AVR system, the AVR structure has been fixed by the Heffron–Philips model of the synchronous generator. This structure is well-known and its good performance has been proved in practice. Also, the deviation intervals of the Heffron–Phillips parameters are specified (Table 1). Consequently, the application of the unstructured uncertainties is quite clear-cut.

In block diagram of Fig. 2, the structure of amplifier, exciter and generator transfer functions are similar. They are one order transfer functions with gain (K_i) and time constant (T_i) real parametric uncertainties where $i \in \{A, E, G\}$. By defining a new gain coefficient ($K_F = K_A K_E K_G$) and assuming a fix transfer function for sensor in its nominal values, there exist four independent parameters (K_F, T_A, T_E, T_G) in the system forward transfer function. On the other hand, by assuming this new gain coefficient (K_F), the six system uncertainties ($K_A, T_A, K_E, T_E, K_G, T_G$) will be reduced to four uncertainties (K_F, T_A, T_E, T_G).

If the nominal values and tolerance percentages of these uncertainties have been conveyed by $\left(\tilde{K}_F, P_{KF}\right)$ and $\left(\tilde{T}_i, P_{Ti}\right)$ respectively, the uncertainties in the structure of upper linear fractional transforming (LFT) can be demonstrated by:

$$\tilde{K}_F = \frac{K_F(\min) + K_F(\max)}{2}, \qquad P_{Kj} = \frac{K_F(\max) - K_F(\min)}{K_F(\max) + K_F(\min)} \tag{4}$$

$$\tilde{T}_i = \frac{T_i(\min) + K_i(\max)}{2}, \qquad P_{Ti} = \frac{T_i(\max) - T_i(\min)}{T_i(\max) + T_i(\min)} \tag{5}$$

$$K_F = \tilde{K}_F \pm \left(\tilde{K}_F \times P_{KF}\right) = \tilde{K}_F\,(1 \pm P_{KF}) = \tilde{K}_F\,(1 + \delta_{KF} P_{KF}) \quad , \quad \delta_{KF} \in [-1\ 1] \tag{6}$$

$$\frac{1}{T_i} = \frac{1}{\tilde{T}_i \pm \left(\tilde{T}_i \times P_{Ti}\right)} = \frac{1}{\tilde{T}_i\,(1 \pm P_{Ti})} = \frac{1}{\tilde{T}_i\,(1 + \delta_{Ti} P_{Ti})} = \frac{1}{\tilde{T}_i} - \frac{P_{Ti}}{\tilde{T}_i}\delta_{Ti}\,(1 + \delta_{Ti} P_{Ti})^{-1}\ ,\ \delta_{Ti} \in [-1\ 1] \tag{7}$$

where δ_{KF} and δ_{Ti} are real parametric uncertainties and $i \in \{A, E, G\}$. The upper LFT representation of K_F and T_i can be offered in δ_{KF} and δ_{Ti}.

$$K_F = F_L(M_{KF}, \delta_{KF}) \quad with \quad M_{KF} = \begin{bmatrix} \tilde{K}_F & 1 \\ \tilde{K}_F P_{KF} & 0 \end{bmatrix} \tag{8}$$

$$\frac{1}{T_i} = F_L(M_{Ti}, \delta_{Ti}) \quad with \quad M_{Ti} = \begin{bmatrix} \frac{1}{\tilde{T}_i} & \frac{-P_{Ti}}{\tilde{T}_i} \\ -1 & -P_{Ti} \end{bmatrix} \quad and \quad i \in \{A, E, G, S\} \tag{9}$$

Fig. 5 shows all of the above LFTs in the block structure.

The block diagram of a first order transfer function $\left(\frac{K_F}{1+T_i s}\right)$ with LFTs block diagram of its uncertainties (K_F , T_i) has been demonstrated in Fig. 6. The AVR's P-Δ representation without the weighting functions can be achieved by substitution of the LFTs block diagrams of the system uncertainties (K_F, T_A, T_E, T_G) in Fig. 6. Fig. 7 shows the required structure to construct the AVR P-Δ-K representation.

In Fig. 7 the AVR system has four uncertainties ($\delta_{KF}, \delta_{TA}, \delta_{TE}, \delta_{TG}$), one reference input ($r$), one disturbance input (d), one noise input (n), one error signal for the controller (e), one input from the controller (c), one terminal voltage (v_t), four perturbation inputs ($p_{i1}\ p_{i2}\ p_{i3}\ p_{i4}$) and four perturbation outputs ($p_{o1}\ p_{o2}\ p_{o3}\ p_{o4}$). By supposing that the AVR system has four states ($x_1 - x_4$), eight inputs and six outputs, it can be shown that the linear state space representation of Fig. 7 is:

$$\begin{cases} \dot{x} = A_{tot}\, x + B_{tot}\, u \\ y = C_{tot}\, x + D_{tot}\, u \end{cases} \tag{10}$$

Which the inputs, outputs and states are $u = [p_{i1}\ p_{i2}\ p_{i3}\ p_{i4}\ r\ d\ n\ c]^T$, $y = [p_{o1}\ p_{o2}\ p_{o3}\ p_{o4}\ v_t\ e]^T$ and $x = [x_1\, x_2\, x_3\, x_4]^T$, respectively. The state space matrices are:

$$A_{tot} = \begin{bmatrix} \frac{-1}{\tilde{T}_A} & 0 & 0 & 0 \\ \frac{1}{\tilde{T}_E} & \frac{-1}{\tilde{T}_E} & 0 & 0 \\ 0 & \frac{1}{\tilde{T}_G} & \frac{-1}{\tilde{T}_G} & 0 \\ 0 & 0 & \frac{K_S}{T_S} & \frac{-1}{T_S} \end{bmatrix} \tag{11}$$

$$B_{tot} = \begin{bmatrix} B_1 & B_2 \end{bmatrix} \tag{12}$$

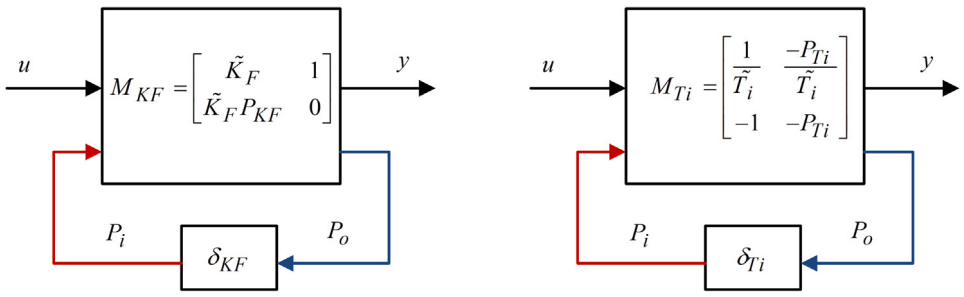

Fig. 5. Representation of uncertain parameters K_F and T_i as LFTs block diagram.

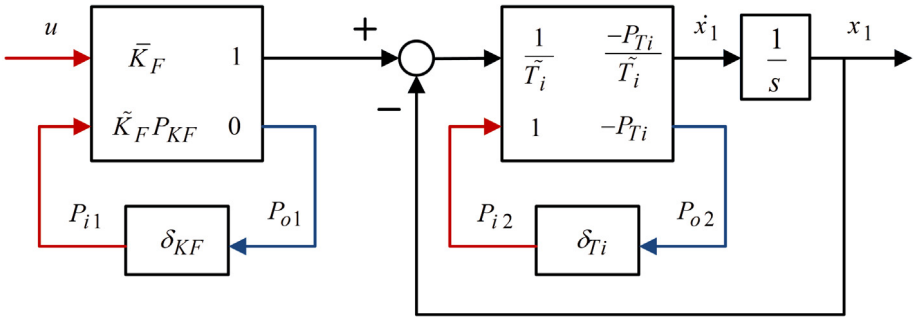

Fig. 6. Block diagram for P-Δ representation of the $K_F/(1+ T_i\ s)$ transfer function with K_F and T_i uncertainties.

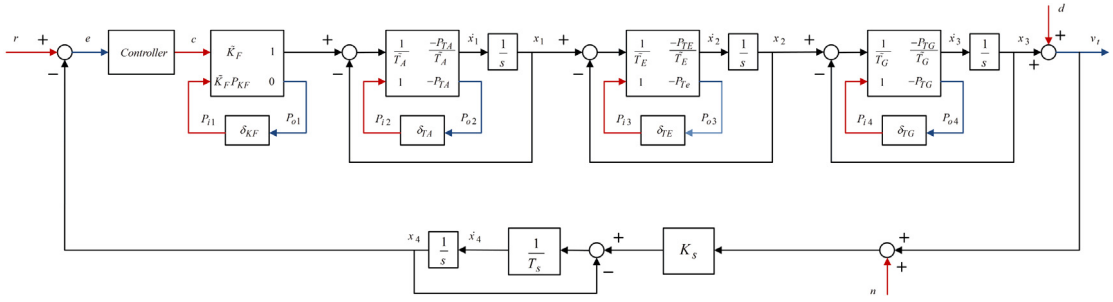

Fig. 7. AVR plant with P-Δ representation of the system uncertainties for μ-synthesis.

$$B_1 = \begin{bmatrix} \frac{1}{\tilde{T}_A} & \frac{-P_{TA}}{\tilde{T}_A} & 0 & 0 \\ 0 & 0 & \frac{-P_{TE}}{\tilde{T}_E} & 0 \\ 0 & 0 & 0 & \frac{-P_{TG}}{\tilde{T}_G} \\ 0 & 0 & 0 & 0 \end{bmatrix}, B_2 = \begin{bmatrix} 0 & 0 & 0 & \frac{\tilde{K}_F}{\tilde{T}_A} \\ 0 & 0 & 0 & 0 \\ 0 & 0 & 0 & 0 \\ 0 & \frac{K_S}{T_S} & 0 & 0 \end{bmatrix} \tag{13}$$

$$C_{tot} = \begin{bmatrix} C_1 \\ C_2 \end{bmatrix} \tag{14}$$

$$C_1 = \begin{bmatrix} 0 & 0 & 0 & 0 \\ -1 & 0 & 0 & 0 \\ 1 & -1 & 0 & 0 \\ 0 & 1 & -1 & 1 \end{bmatrix}, C_2 = \begin{bmatrix} 0 & 0 & 1 & 0 \\ 0 & 0 & 0 & -1 \end{bmatrix} \tag{15}$$

$$D_{tot} = \begin{bmatrix} D_{11} & D_{12} \\ D_{21} & D_{22} \end{bmatrix} \tag{16}$$

$$D_{11} = \begin{bmatrix} 0 & 0 & 0 & 0 \\ 0 & -P_{TA} & 0 & 0 \\ 0 & 0 & -P_{TE} & 0 \\ 0 & 0 & 0 & -P_{TG} \end{bmatrix} \tag{17}$$

$$D_{12} = \begin{bmatrix} 0 & 0 & 0 & \tilde{K}_F P_{KF} \\ 0 & 0 & 0 & \tilde{K}_F \\ 0 & 0 & 0 & 0 \\ 0 & 0 & 0 & 0 \end{bmatrix} \tag{18}$$

$$D_{21} = \begin{bmatrix} 0 & 0 & 0 & 0 & 0 & 0 \\ 0 & 0 & 0 & 0 & 0 & 0 \end{bmatrix} \tag{19}$$

$$D_{22} = \begin{bmatrix} 0 & 1 & 0 & 0 \\ 1 & 0 & 1 & 0 \end{bmatrix} \tag{20}$$

The P-Δ-K representation of the AVR system without weighting functions is shown in Fig. 8 where the AVR plant (*AVR_Plant*) has the state space equations of (10)–(20) and $\Delta = diag(\delta_{KF}, \delta_{TA}, \delta_{TE}, \delta_{TG})$ is a 4×4 structured uncertainty. It is a diagonal matrix and has a fixed structured such that its elements belong to $[-1, 1]$ interval.

5. P-Δ-K representation of the AVR plant with weighting functions

Fig. 9 shows the system closed-loop in the presence of the structured diagonal uncertainty and weighting functions blocks. W_p is the performance weighting function for the output voltage of the generator and bounds the system's sensitivity function

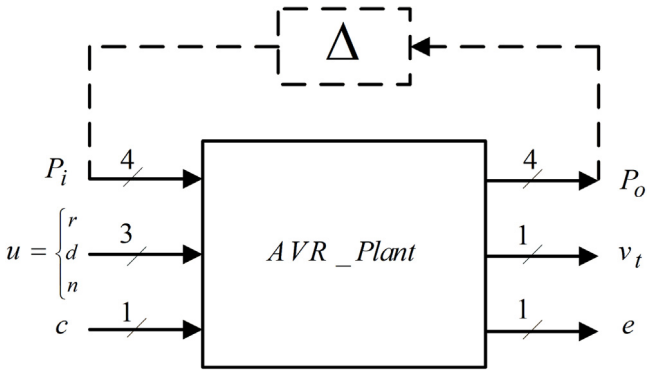

Fig. 8. P-Δ-K representation of the AVR system without weighting functions.

$\left(S(s) \leq W_s^{-1}(s)\right)$ to create the possible small sensitivity output disturbances as:

$$W_p(s) = \frac{K_{wp}\left(\frac{s}{M_p} + \omega_p\right)}{\left(s + \varepsilon_p \omega_p\right)} = \frac{\left(\frac{s}{10} + 2\sqrt{2}\right)}{100\left(s + 0.02\sqrt{2}\right)} \tag{21}$$

On the other hand, for confining the control system energy, the control weighting functions (W_u) have been selected to decrease the magnitude of the controller outputs. The following structure has been chosen for W_u.

$$W_u(s) = \frac{K_{wu}\left(s + \frac{\omega_u}{M_u}\right)}{\left(\varepsilon_u s + \omega_u\right)} = \frac{\left(s + \frac{0.01}{100}\right)}{100\left(0.01s + 20000\sqrt{2}\right)} \tag{22}$$

Fig. 10 shows the magnitude curve of the reverse of the performance function $\left(W_p^{-1}\right)$ and control weighting function (W_u).

6. Designing the suboptimal H_∞ controller

After introducing the P-Δ-K representation of the AVR system (as shown in Fig. 9), its nominal plant (AVR_nom) can be constructed easily. After that, the suboptimal H_∞ controller is sketched by the nominal plant of the AVR_ic (AVR_nom). This nominal plant (AVR_nom) has four inputs $\left(\left[ref \quad dist \quad noise \quad c\right]\right)$ and three outputs. The SISO suboptimal controller minimizes the infinity norm of the $F_L(AVR\_nom, K)$ overall SISO stabilizing controllers (K) as Eq. (23). $AVR_cl = F_L(AVR_nom, K)$is the LFT of the nominal system and the designed suboptimal H_∞ controller.

$$\gamma_0 = \min_{K(s)} \|T_{zw}\|_\infty = \min_{K(s)} \|F_L(AVR\_nom, K(s))\|_\infty$$
$$=< \gamma < 1 \quad Where \quad z = \begin{bmatrix} y \\ y_c \end{bmatrix}, w = \begin{bmatrix} ref \\ dist \\ noise \end{bmatrix} \tag{23}$$

Fig. 11 shows the AVR nominal plant and its LFT representation with the controller (K) which has been designed by H_∞ optimization in MATLAB using Glover and Doyle [59] method for a system P. Furthermore, this method determines the final gamma value achieved in controller design procedure and constructs the system closed-loop system representation (LFT of the AVR_nom and obtained H_∞ controller or AVR_cl). The proposed strategy could be expanded to any power system easily by the below procedure and the flowchart of Fig. 12.

1– Running the load flow analysis for the intended system and calculating the reactive power, active power, and terminal voltage of a specific generator.

2– Computing the time constant and gain of the specific generator in the operating point based on the values of step1.

3– Constructing the P-Δ-K model of the specified generator by using the proposed equations (Eqs. (10)–(20)).

4– Creating the P-Δ −K depiction of the AVR system (Fig. 9) with the usage of the introduced weighting functions (Eqs. (21) and (22)).

5– Designing the H infinity controller for the P-Δ-K representation of step 4 (minimizing Eq. (23)).

6– Evaluating the robust performance and stability of the closed-loop P−Δ−K representation (Fig. 9 in combination with the Δ and designed controller blocks) by Mu theorem.

On the basis of the above procedure and the data of Table 1, a six order SISO controller has been obtained like as Eq. (24) (see Box I) which its closed pole to the origin (s = −0.0173) is converted to an origin pole (s = 0). The bode diagram of this appropriate controller is represented in Fig. 13.

For the case presented, the amount of $\|F_L(AVR\_nom, K)\|_\infty = \|AVR\_cl\|_\infty$ or γ is 0.2001. Since the AVR plant uncertainties have been considered as structured, authentication of the system robust stability (RS) and robust performance (RP) need checking the frequency response of $F_U\left(AVR\_ic, \tilde{\Delta}\right)$ based on μ values. By defining the $\tilde{\Delta}$ block as (25), the robust performance (RP) of the designed system is obtained, if and only if $\mu_{\tilde{\Delta}}(\cdot) < 1$ for each

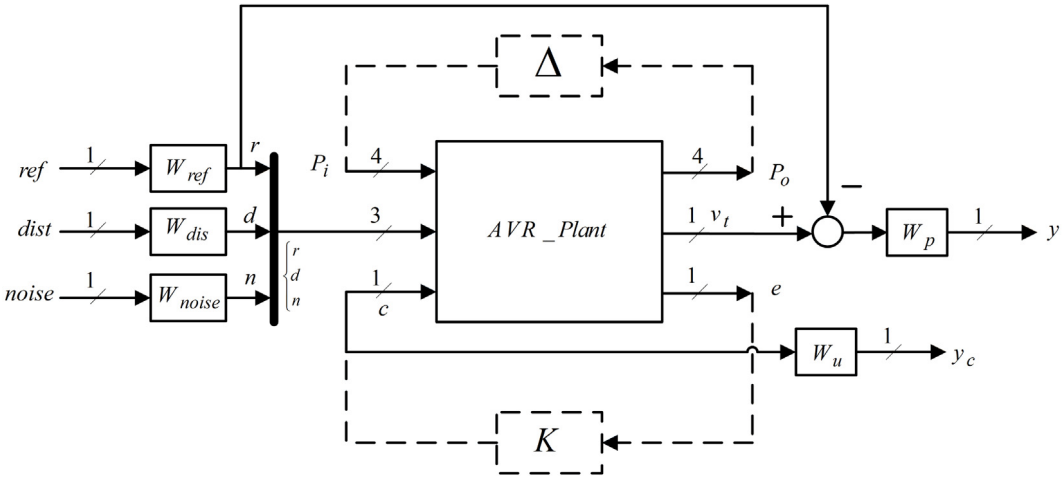

Fig. 9. The AVR closed-loop system diagram with structured diagonal uncertainty block and weighting functions.

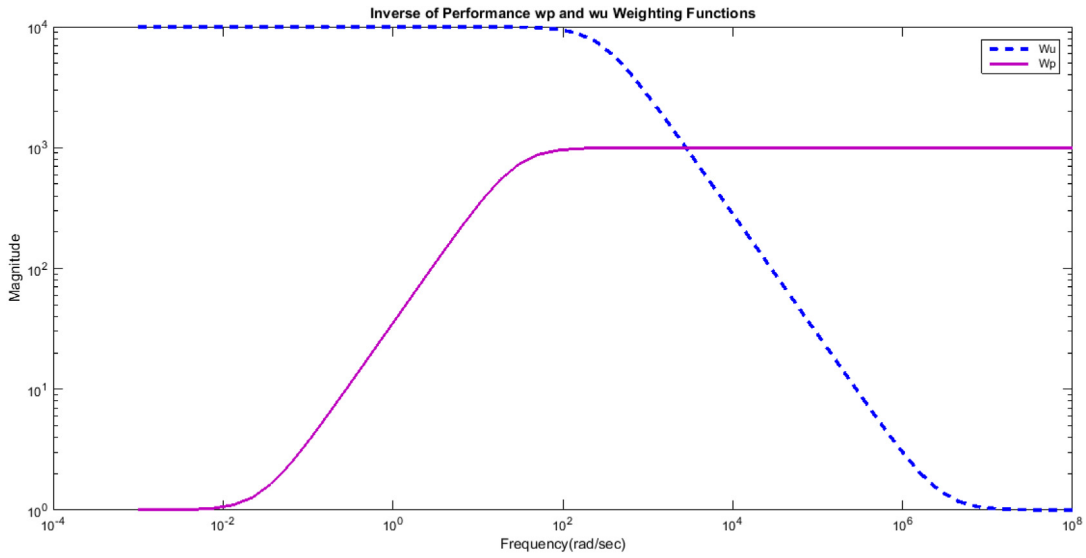

Fig. 10. The magnitude plot of inverse of the performance (W_p) and the control weighting (W_u) functions.

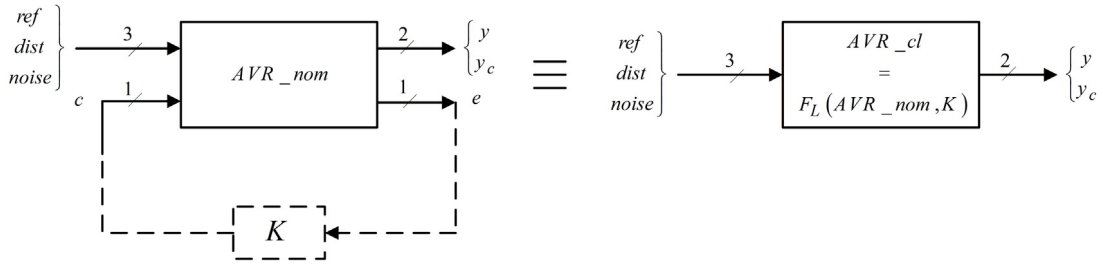

Fig. 11. AVR nominal plant and its LFT representation with the designed H_∞ controller (K).

$$K(s) = \frac{0.02883s^5 + 81562.8s^4 + 703621s^3 + 15750024.5s^2 + 48471744s + 33417184.4}{s^6 + 222.7s^5 + 22584s^4 + 1372617s^3 + 53530000s^2 + 1263000000s} \tag{24}$$

Box I.

frequency.

$$\tilde{\Delta} := \left\{ \begin{bmatrix} \Delta & 0 \\ 0 & \Delta_P \end{bmatrix} : \Delta \in \mathbb{R}^{4\times 4},\ \Delta_P \in \mathbb{C}^{3\times 2} \right\} \tag{25}$$

Fig. 14 shows the upper linear fractional of the closed loop system by existing the structured and unstructured uncertainties $\left(F_U\left(AVR\_ic\ ,\ \tilde{\Delta}\right)\right)$. The frequency response of $\mu_{\tilde{\Delta}}\left(F_U\left(AVR\_ic, \tilde{\Delta}\right)\right) < 1$ reflecting the robust and nominal performance is provided in Fig. 15.

7. Simulation of the linear AVR system in five scenarios

In this section, some scenarios have been considered to show the merit of the robust performance of the designed controller. These scenarios have been adopted based on the nominal values, maximum values, minimum values and the tolerance percentages of the system uncertainties by existing the output disturbance. The designed H_∞ controller performance is evaluated with 5 different controllers as follow:

1– A conventional PID controller enhanced by Teaching–Learning based Optimization Technique [14].
2– A PID plus second order derivative controller optimized by PSO algorithm (PIDD2) [33]
3– A PID fractional order controller enhanced by cuckoo search based algorithm [30] and was implemented by a 28-order linear transfer function (N = 6) with FOMCOM toolbox for MATLAB (version 1.21b) [63].
4– A fuzzy+ PID controller [31] based on the MATLAB fuzzy logic system toolbox and optimized by TLBO algorithms.
5– A type2 fuzzy controller in term of the interval type2 fuzzy logic system toolbox (IT2FLS) [64].

The absolute majority of these AVR controllers have been designed based on small gain and large time constant of the amplifier, exciter, generator and sensor [7,9,17–19,25,33]. The AVR characteristics are: $K_A = 10$, $K_E = 1$, $K_G = 1$, $K_S = 1$, $T_A = 0.1$, $T_E = 0.4$, $T_G = 1$ and $T_S = 0.01$. The closed loop system with these parameters is stable and the controller only modifies the performance of it. Whereas, in nominal point ($K_A = 25$, $K_E = 5.5$, $K_G = 0.85$, $K_S = 1$, $T_A = 0.06$, $T_E = 0.7$, $T_G = 1.5$, $T_S = 0.0305$) the closed loop system without controller is unstable and has two poles in the right half plane (3.1565 ± 10.4205i). Since increasing the gain and the speed of the AVR system makes reaching to the stability hard, this problem will become more ambiguous when the gains are increased and the time constants are decreased. Therefore, designing the controller at this nominal point is harder and optimized controllers

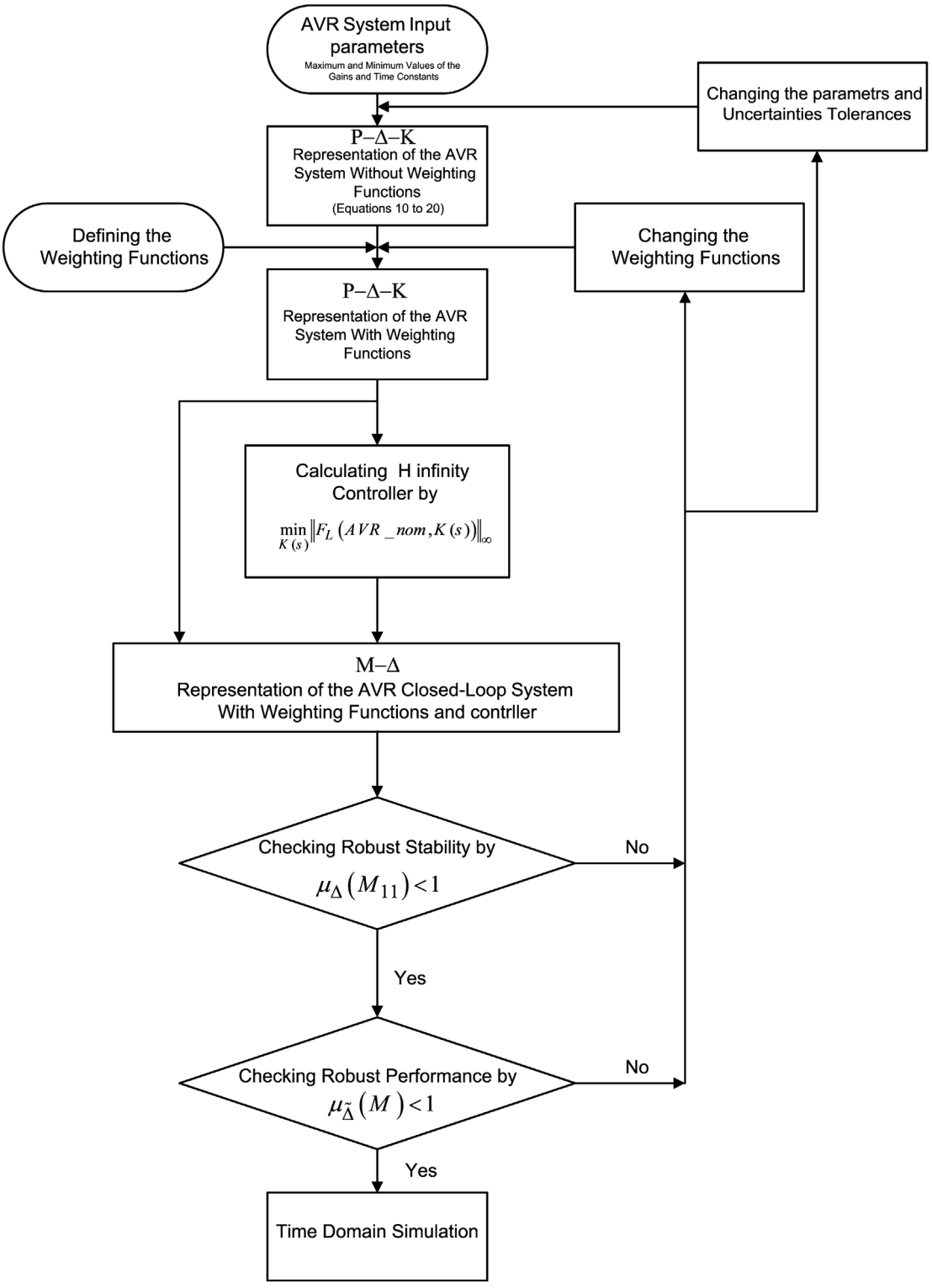

Fig. 12. The flowchart of the robust H_∞ controller design procedure for the AVR system in a large size power system.

by optimization algorithms cannot perform best at this condition. The simulation results justify this claim and show that these optimized controllers only have a good performance around their base plant.

In all simulations, this pattern has been considered to assess the controllers' performance:

1. There is a 1^{pu} change in the reference voltage at $t = 0$ for analyzing the tracking performance.
2. In order to analyze short circuit faults, the generator's terminal voltage will be zero by a -1^{pu} sudden disturbance at the output terminal voltage. In this case, the controllers must return the output voltage to the reference value.
3. By a sudden increment in the terminal voltage to 2^{pu}, the transient overvoltage can be modeled. For this modeling

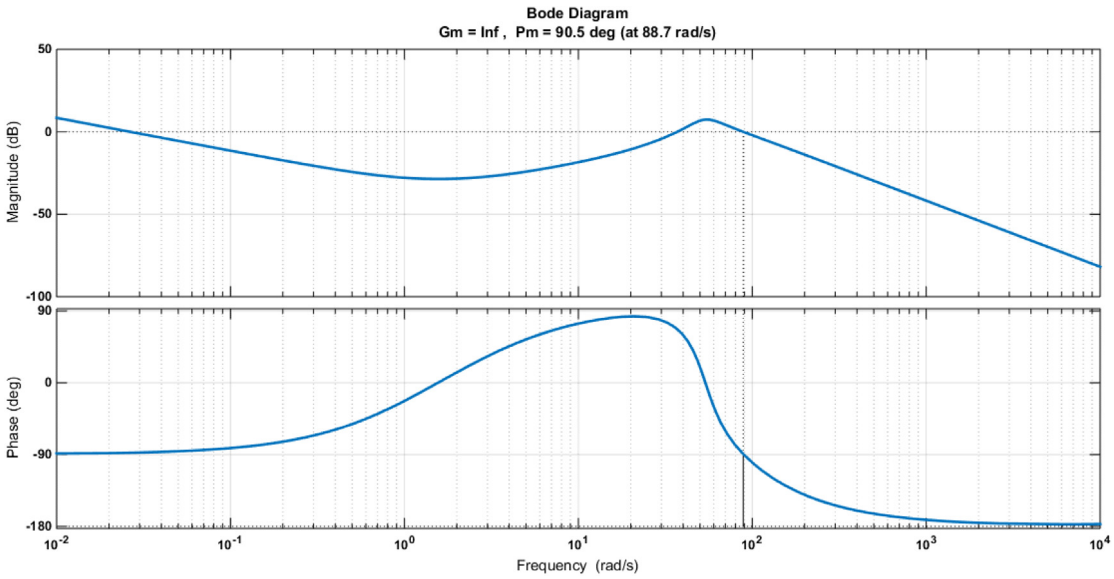

Fig. 13. Bode diagram of the designed H_∞ controller *(K)*.

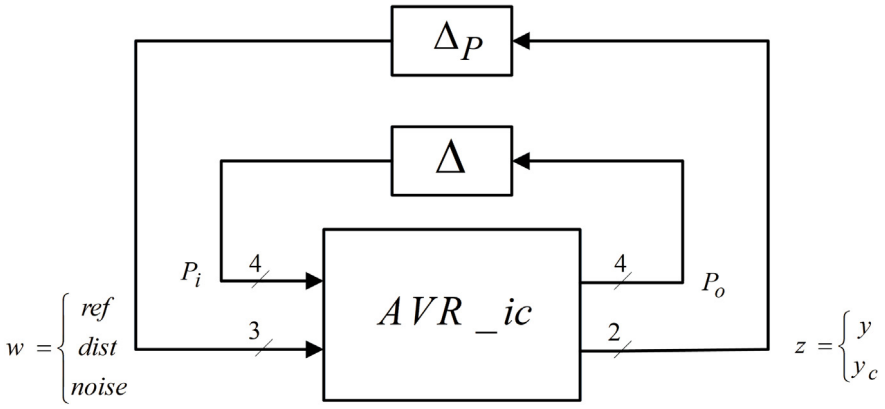

Fig. 14. Upper linear fractional of the closed loop system in the presence of the structured and unstructured uncertainties.

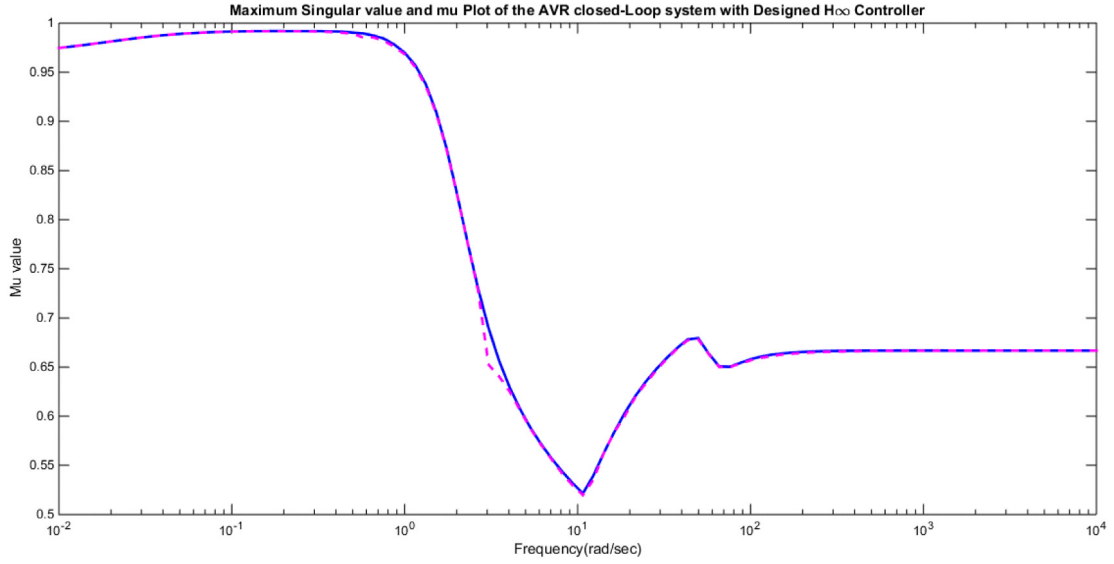

Fig. 15. Robust performance of the suboptimal H_∞ controller.

a 1^{pu} voltage disturbance has been added to the terminal voltage.

These patterns are applied to the AVR system in five points of functional area according to the following five scenarios:

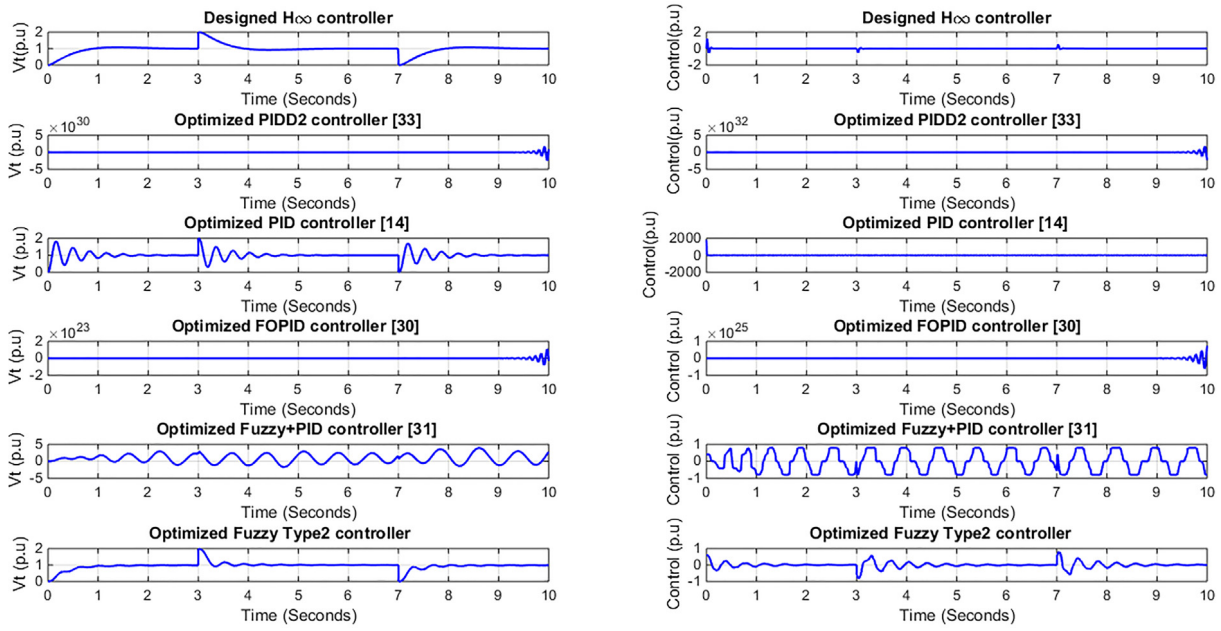

Fig. 16. Performance of the controllers in scenario #1 (nominal values of uncertainties).

1– The nominal values of time constants and gains of the transfer functions.

2– The maximum values of time constants and gains of the transfer functions.

3– The minimum values of time constants and gains of the transfer functions.

4– The maximum values of gains and minimum values of time constants of the transfer functions.

5– The minimum values of gains and maximum values of time constants of the transfer functions.

Since the performance of the controllers is different in these five scenarios, the applying time of pattern #2 and pattern #3 in these scenarios are not the same. For instance, in scenario #1, pattern #2 has been applied in t = 3 s and pattern #3 has been applied in t = 7 s. In scenario #2 these times are t = 7 s and t = 10 s, respectively.

7.1. Scenario #1: nominal values of uncertainties

In the first scenario, the amplifier, the exciter, and the generator parameters have been set at their nominal values ($K_A = 25,\ K_E = 5.5,\ K_G = 0.85,\ K_S = 1,\ T_A = 0.06,\ T_E = 0.7,\ T_G = 1.5, T_S = 0.0305$). Fig. 16 shows the generator terminal voltage and output controller effort where the fractional order and PIDD^2 controller is unstable and the PID controller has not good transient characteristics.

7.2. Scenario #2: maximum values of uncertainties

In the second scenario, the amplifier, the exciter, and the generator parameters have been set at their maximum values ($K_A = 40, K_E = 10, K_G = 1, K_S = 1, T_A = 0.1, T_E = 1, T_G = 2,\ T_S = 0.0305$). Fig. 17 shows the generator terminal voltage and output controller effort where the fractional order, PIDD^2 and PID controllers are unstable and the overshoot and settling time of the H_∞ controller have been increased in comparison with the previous case.

7.3. Scenario #3: minimum values of uncertainties

In the third scenario, the amplifier, the exciter, and generator parameters have been set at their minimum values ($K_A = 10, K_E = 1,\ K_G = 0.7,\ K_S = 1,\ T_A = 0.02,\ T_E = 0.4,\ T_G = 1, T_S = 0.0305$). Fig. 18 shows the generator terminal voltage and output controller effort where the transient behavior of the PIDD^2 controller is bad and both fractional order and PID controllers have good performances because this scenario is close to the working point in which these controllers have been optimized. In this scenario, the act of the robust controller is close to these controllers.

7.4. Scenario #4: system gains are maximum and time constants are minimum

In the fourth scenario, the amplifier, the exciter, and the generator parameters have been set at: $K_A = 40, K_E = 10,\ K_G = 1,\ K_S = 1,\ T_A = 0.02,\ T_E = 0.4,\ T_G = 1, T_S = 0.0305$. Fig. 19 shows the generator terminal voltage and output controller effort where the fractional order, PIDD^2 and PID controllers are unstable but the speed and steady state error of the robust controller is so good.

7.5. Scenario #5: system gains are minimum and time constants are maximum

In the fifth scenario, the amplifier, the exciter, and the generator parameters have been set at: $K_A = 10, K_E = 1,\ K_G = 0.7,\ K_S = 1,\ T_A = 0.1,\ T_E = 1,\ T_G = 2, T_S = 0.0305$. Fig. 20 shows the generator terminal voltage and output controller effort where the systems functions are the same as the scenario #3.

In scenarios #3 and #5 where the gains of the transfer functions are at minimum, the behavior of the PID and fractional order controller look like the H_∞ controller. However, this fact is based on their unacceptable control effort. These controllers have been designed close to the minimum values of uncertainties [14,30]. Therefore, the performance of these controllers in scenarios #3 and #5 (minimum values of the uncertainties) is good because they have been optimized around these minimum points.

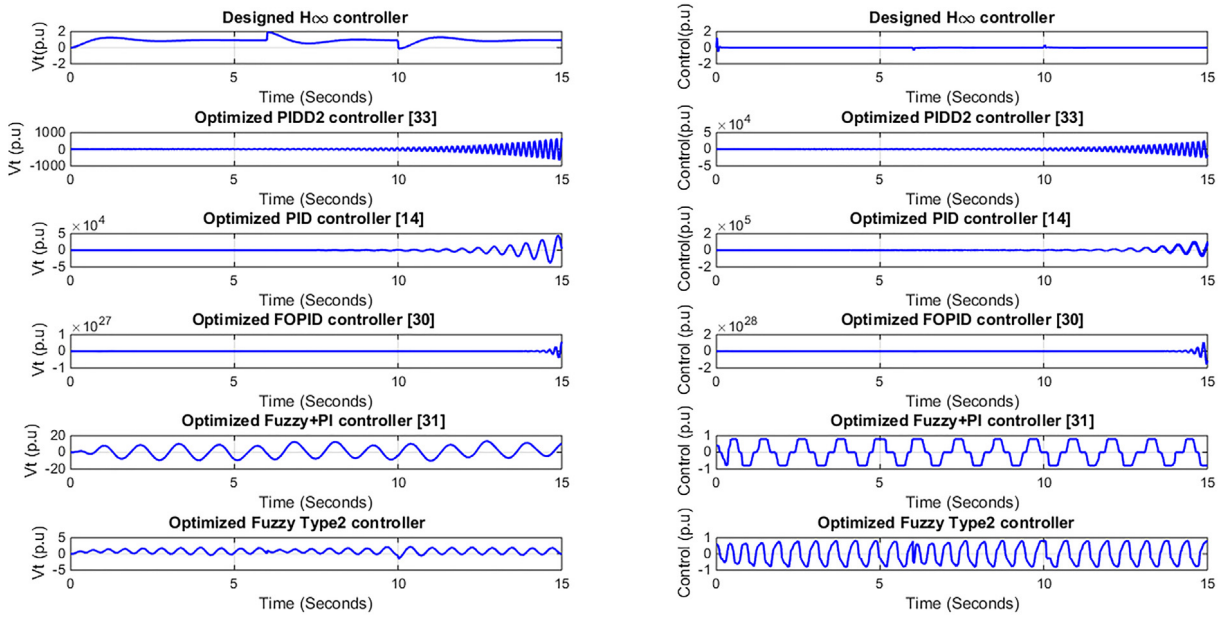

Fig. 17. Performance of the controllers in scenario #2 (maximum values of uncertainties).

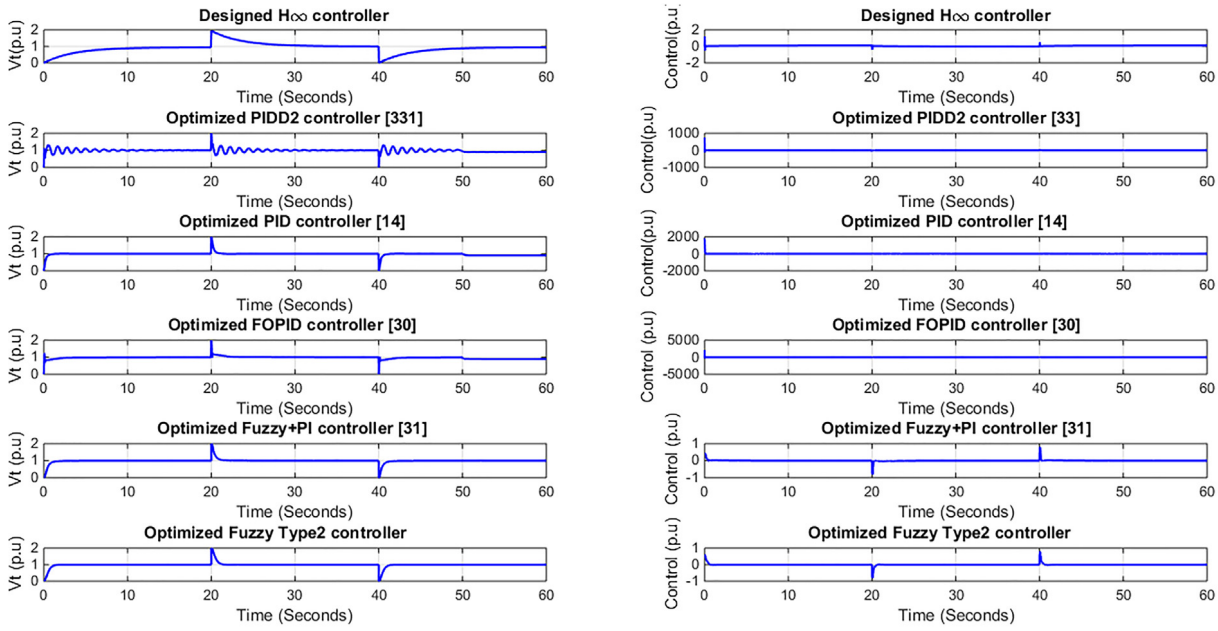

Fig. 18. Performance of the controllers in scenario #3 (minimum values of uncertainties).

On the other hand, in robust controller design procedure, we have considered a weighting function (W_u) to limit the control effort. This limitation causes the gain of the robust controller to become so small in all scenarios. The limitation of the controller output effort is one of the most important achievements of the robust controller. If the simulation results of the other three controllers are reckoned in scenarios, it can be easily seen that their controller output amplitude is very large and unacceptable.

8. Simulation a real synchronous generator connected to a 230 kV network [65,66]

In this section, a 200 MVA, 13.8 kV, 112.5 rpm generator has been studied which is linked to a 230 kV network via a Delta-Y 210 MVA transformer. Fig. 21 shows this connection. The system initiates in steady state with the generator supplying 150 MW of active power. At t = 0.1 s, a three-phase to ground fault occurs on the 230 kV bus of the transformer. The fault is cleared followed by 6 cycles [65,66]. The synchronous generator has been modeled by 7-order nonlinear equations and has a separated LFC control system (governor, turbine, and PID frequency controller). To show the merit of our designed robust controller, its transfer function Eq. (24) with the amplifier and exciter has been substituted instead of the original AVR controller (IEEE standard) without any change in the system structure and parameters. Fig. 22 represents the deviation of the voltage terminal magnitude by these two controllers. Although our robust controller has not been designed strictly for this system, its performance is obviously better than the IEEE standard exciting system (controller + amplifier + exciter). If the synchronous generator parameters have been

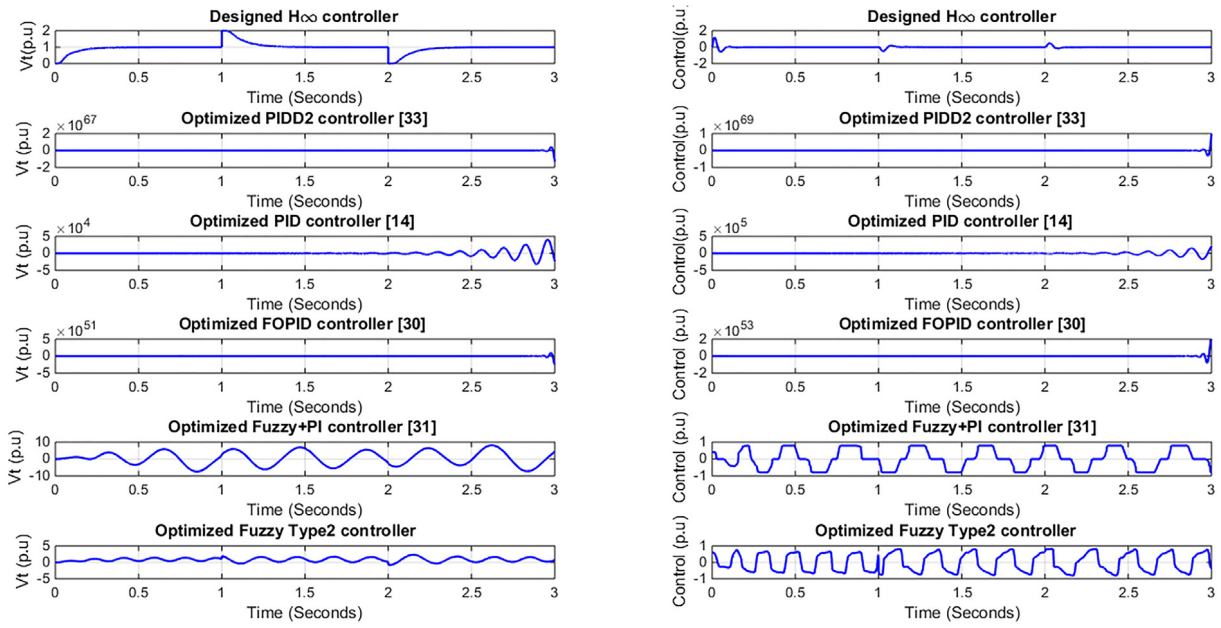

Fig. 19. Performance of the controllers in scenario #4 (the system gains are maximum and the time constants are minimum).

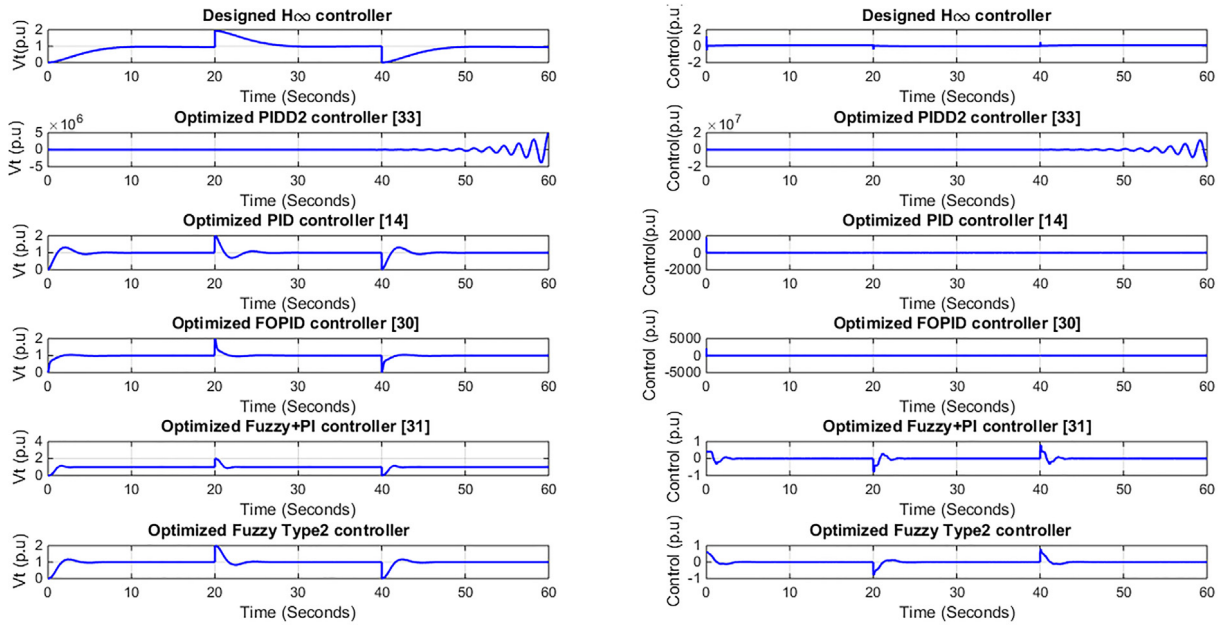

Fig. 20. Performance of the controllers in scenario #5 (the system gains are minimum and the time constants are maximum).

considered and the gain and time constant of its 1-order model computed, the H infinity controller could be designed perfectly for this system by using the P-Δ-K generator representation which has been introduced in paper.

9. Comparison the generic power system stabilizer and designed robust controller in the four-machine two-area test system [2,67–69]

Fig. 23 represents the benchmark system including 2 quite symmetric areas connected together by two 230 kV lines of 220 km length. It was precisely introduced in [68] and [2] to investigate low frequency oscillations in large interconnected power systems. Contrary to its small size, it patterns very nearly the action of the systems in real operation [68]. Each area has been armed with two similar generators rated 20 kV/900 MVA. The M1 and M2 tools are in area 1 and M3 and M4 machines are in area 2, respectively (Fig. 23). The synchronous generators have equal characteristics [2,68] excepts for inertias which are H = 6.5 s in area 1 and H = 6.175 s in area 2 [2]. Constant impedances have been considered as the load of the system. They are distributed between the two areas in which 413 MW active power is exported from area 1 to area 2.

In the simulation process, the robust AVR controller Eq. (24) is considered as our designed robust controller for the AVR subsystem of Fig. 23. This block has been substituted instead of the multiband (MB) PSS, Delta pa PSS, and Delta W PSS controllers of the main system [67,68]. Three scenarios are considered to evaluate the performance of the controllers.

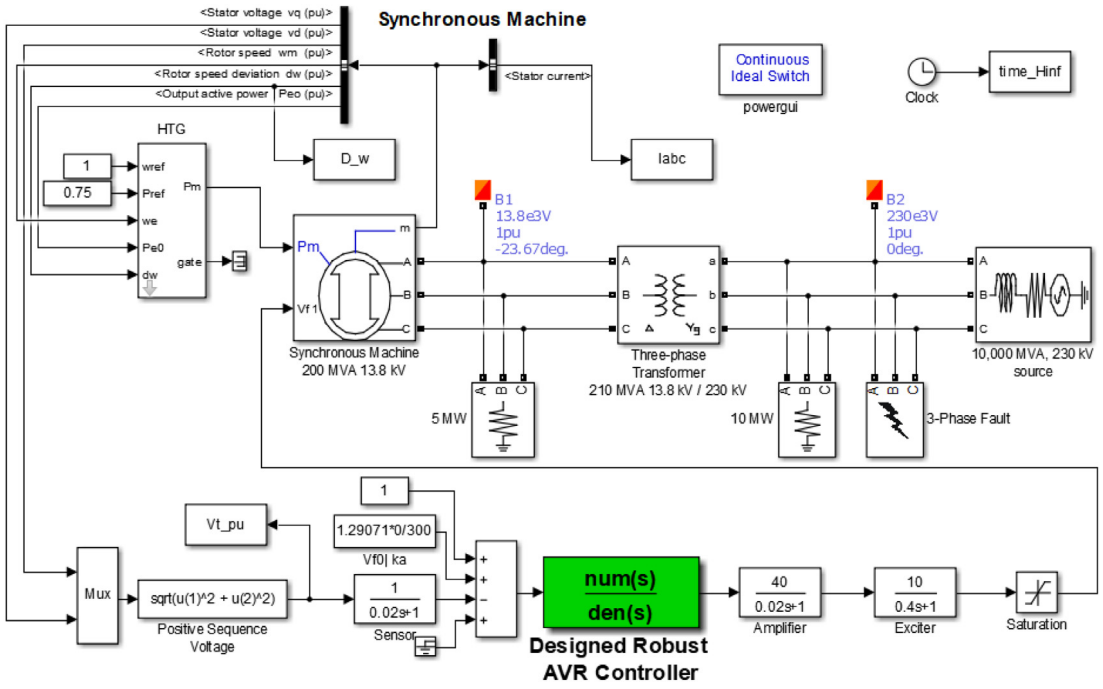

Fig. 21. The Synchronous Machine associated with the Hydraulic Turbine and Governor (HTG) and Excitation System (AVR) [65].

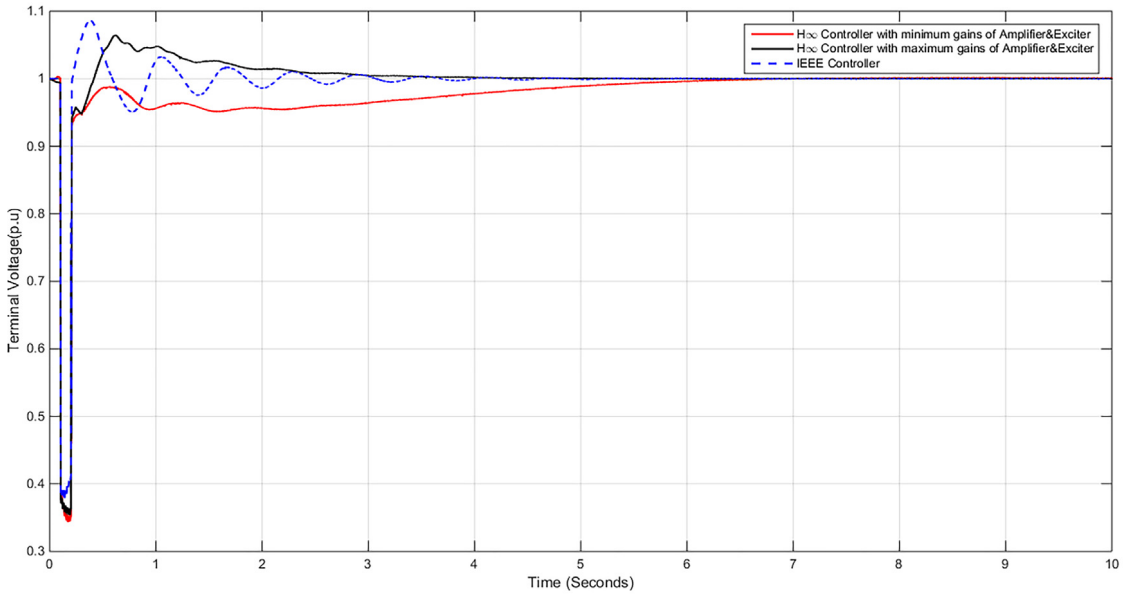

Fig. 22. The terminal voltage of the synchronous machine in 230 KV networks.

(a) For simulating the small-signal closed-loop system responses, a 6-cycle pulse for 5 percent change on voltage reference of M1 is applied in time of 5 s. On the other hand, at the time of 5 s the reference voltage of the generator M1 has been changed from 1 p.u to 1.05 p.u for 0.1 s.

(b) The outage of one 230 KV line by adjusting the breakers "Brk1" and "Brk2" in an open condition at the time of 20 s for 8 cycles. Without one tie-line, the system can reach a stable operating point in steady-state but the voltage controller or PSS must guarantee a smooth transition into this novel greatly stressed operating point.

(c) A three-phase short circuit fault in 230 KV line #1 and a one-phase short circuit fault in 230 KV line #2 will be occurred at time 40 s for 0.1 s. Good performance over large perturbations and good robustness in the regard of altering the operating circumstances are other criteria of an equal importance.

Fig. 24 shows the terminal voltage of the synchronous generator number 4 (M4) based on designed robust controller and three types of proposed PSS [67,68]. Obviously, the transient and steady-state response of the closed loop system with the robust controller is much better.

10. Conclusion

In this work, robust H_∞ and μ-analysis methods have been used to set the synchronous generator's terminal voltage. To apply these robust control methods, the P-Δ-K representation

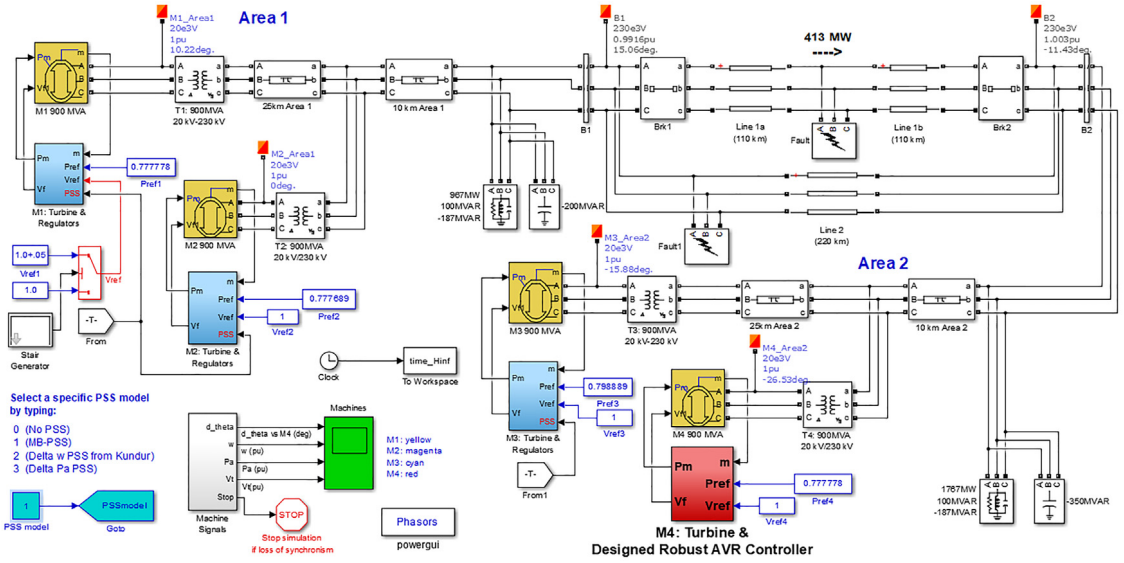

Fig. 23. The test system of two fully symmetrical areas linked together by two 230 kV lines of 220 km length [67,68].

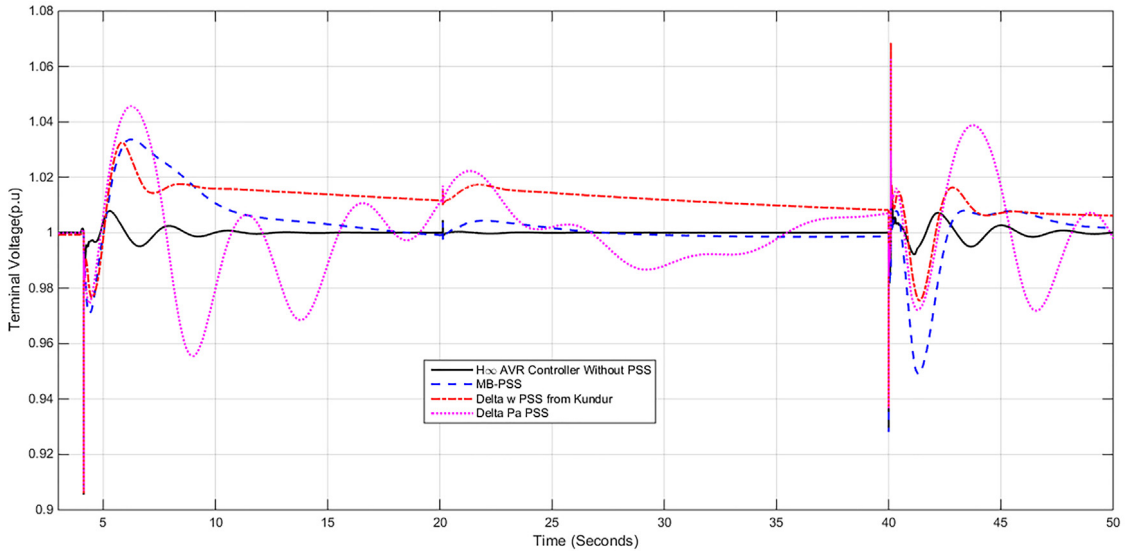

Fig. 24. The terminal voltage of the synchronous generator number 4 based on designed robust controller and three types of proposed PSS [67,68].

must be derived from the system model and its uncertainties. By defining a new gain coefficient as AVR gain which is equal to the multiplication of the gain coefficients of the exciter, the amplifier and the generator, the system has four real structured parameters. Furthermore, all the system real structured factors have been modeled by nominal values and percentage variations have been determined based on their minimum and maximum values (the AVR gain and amplifier time constant parameter have 96% and 66% tolerance, respectively). These large deviations and the four real structured uncertainties cause the H_∞ and μ-analysis procedures to be complicated. After obtaining the M-Δ model of any parameters of the AVR, the P-Δ-K representation of it has been constructed without any conservation in the presence of the AVR dynamic perturbations and some weighting functions. A H_∞controller has been designed based on this representation, to decrease the impacts of generator output disturbance and reference voltage tracking. The μ value of the closed loop system satisfies the robust performance condition $\left(\mu_{\tilde{\Delta}}(M) < 1\right)$.

The merit of the suggested H_∞ controller has been exhibited by time domain simulation in MATLAB and Simulink for three case studies. The simulation results of the five scenarios of the AVR linear system show that the accomplishment of the propounded robust controller for the AVR system is superior to the some other optimized PID, PIDD^2, fractional order PID (FOPID), fuzzy + PID and Interval Type-2 fuzzy logic controllers by heuristic optimization algorithms. Although, these controllers have a better performance in minimum values of the system parameters, but they are not stable in more points of the system operation particularly when the gain of AVR is high. This matter stems from this fact that these controllers have been optimized around a base working point which is near the minimum values of the system parameters. Moreover, the PID, PIDD^2 and FOPID controllers have a high oscillation in nominal points of operation and a high unacceptable output control effort in the whole of the uncertainties interval. Also, the better performance of the designed robust controller in a single machine connected to a 230 kV network and the Four-Machine Two-Area Test System has been shown.

Based on the proposed approach for the AVR system with structured uncertainties as P-Δ-K representation, it may be expanded by some other robust controller design manners. In the future works, it could be tried to design some new robust controllers based on μ-synthesis DK iteration, mixed loop-shaping, and quantitative feedback theory (QFT), to improve the new robust control design approach.

Declaration of competing interest

The authors declare that they have no known competing financial interests or personal relationships that could have appeared to influence the work reported in this paper.

References

[1] Padiyar KR. Power system dynamics: stability and control. BS Publications; 2008.
[2] Kundur P. Power system stability and control. 1st ed. New York: McGraw-Hill; 1994.
[3] Demello FP, Concordia C. Concepts of synchronous machine stability as affected by excitation control. IEEE Trans Power Appar Syst 1969;PAS-88:316–29. http://dx.doi.org/10.1109/TPAS.1969.292452.
[4] Ang K, Chong G, Li Y. PID control system analysis, design, and technology. Control Syst Technol IEEE Trans 2005;13:559–76. http://dx.doi.org/10.1109/tcst.2005.847331.
[5] Thangavelusamy D, Ponnusamy L. Study and comparison of PI controller tuning techniques using bacteria foraging and bacteria foraging based particle swarm optimization. Int J Electr Eng 2012;5:571–86.
[6] Gaing ZL. A particle swarm optimization approach for optimum design of PID controller in AVR system. IEEE Trans Energy Convers 2004;19(2):384–91. http://dx.doi.org/10.1109/TEC.2003.821821.
[7] Gozde H, Taplamacioglu MC. Comparative performance analysis of artificial bee colony algorithm for automatic voltage regulator (AVR) system. J Franklin Inst 2011;348:1927–46. http://dx.doi.org/10.1016/j.jfranklin.2011.05.012.
[8] Shirvani M, Shakeri P, Behzadipour E, Baghbani I. PID power system stabilizer design based on Shuffled Frog Leaping algorithm. Life Sci J 2012;9:1071–6.
[9] Panda S, Sahu BKK, Mohanty PKK. Design and performance analysis of PID controller for an automatic voltage regulator system using simplified particle swarm optimization. J Franklin Inst 2012;349:2609–25. http://dx.doi.org/10.1016/j.jfranklin.2012.06.008.
[10] Hasanien HM. Design optimization of PID controller in automatic voltage regulator system using Taguchi Combined Genetic algorithm method. IEEE Syst J 2013;7:825–31. http://dx.doi.org/10.1109/JSYST.2012.2219912.
[11] Mohanty PK, Sahu BK, Panda S. Tuning and assessment of proportional–integral–derivative controller for an automatic voltage regulator system employing local unimodal sampling algorithm. Electr Power Compon Syst 2014;42:959–69. http://dx.doi.org/10.1080/15325008.2014.903546.
[12] Abbasi R, Gholizade H, Molaei B. Optimum design of automatic voltage regulator based on PID controller using imperialistic competition algorithm. J Automot Appl Mech 2015;3.
[13] Priyambada S. Automatic voltage regulator using TLBO algorithm optimized PID controller. In: Ind. inf. syst., 9th int. conf.. Gwalior: IEEE; 2014, p. 1–6. http://dx.doi.org/10.1109/ICIINFS.2014.7036595.
[14] Chatterjee S, Mukherjee V. Electrical power and energy systems PID controller for automatic voltage regulator using teaching–learning based optimization technique. Int J Electr Power Energy Syst 2016;77:418–29. http://dx.doi.org/10.1016/j.ijepes.2015.11.010.
[15] Shayeghi H, Younesi A, Hashemi Y. Optimal design of a robust discrete parallel FP + FI + FD controller for the automatic voltage regulator system. Int J Electr Power Energy Syst 2015;67:66–75. http://dx.doi.org/10.1016/j.ijepes.2014.11.013.
[16] Devaraj D, Selvabala B. Real-coded genetic algorithm and fuzzy logic approach for real-time tuning of proportional-integral - derivative controller in automatic voltage regulator system. Gener Transm Distrib IET 2009;3:641–9. http://dx.doi.org/10.1049/iet-gtd.2008.0287.
[17] Pan I, Das S. Chaotic multi-objective optimization based design of fractional order PIlDm controller in AVR system. Int J Electr Power Energy Syst 2012;43:393–407. http://dx.doi.org/10.1016/j.ijepes.2012.06.034.
[18] Pan I, Das S. Frequency domain design of fractional order PID controller for AVR system using chaotic multi-objective optimization. Int J Electr Power Energy Syst 2013;51:106–18. http://dx.doi.org/10.1016/j.ijepes.2013.02.021.
[19] Tang Y, Cui M, Hua C, Li L, Yang Y. Optimum design of fractional order PIlDm controller for AVR system using chaotic ant swarm. Expert Syst Appl 2012;39:6887–96. http://dx.doi.org/10.1016/j.eswa.2012.01.007.
[20] Zamani M, Karimi-Ghartemani M, Sadati N, Parniani M. Design of a fractional order PID controller for an AVR using particle swarm optimization. Control Eng Pract 2009;17:1380–7. http://dx.doi.org/10.1016/j.conengprac.2009.07.005.
[21] Ramezanian H, Balochian S, Zare A. Design of optimal fractional-order PID controllers using particle swarm optimization algorithm for automatic voltage regulator (AVR) system. J Control Autom Electr Syst 2013;24:601–11. http://dx.doi.org/10.1007/s40313-013-0057-7.
[22] Aguila-Camacho N, Duarte-Mermoud MA. Fractional adaptive control for an automatic voltage regulator. ISA Trans 2013;52:807–15. http://dx.doi.org/10.1016/j.isatra.2013.06.005.
[23] Zhang D-L, Tang Y-G, Guan X-P. Optimum design of fractional order PID controller for an AVR system using an improved artificial bee colony algorithm. Acta Autom Sin 2014;40:973–9. http://dx.doi.org/10.1016/S1874-1029(14)60010-0.
[24] Das S, Pan I. On the mixed H2/H∞ loop-shaping tradeoffs in fractional-order control of the AVR system. IEEE Trans Ind Informatics 2014;10:1982–91. http://dx.doi.org/10.1109/TII.2014.2322812.
[25] Tang Y, Zhao L, Han Z, Bi X, Guan X. Optimal gray PID controller design for automatic voltage regulator system via imperialist competitive algorithm. Int J Mach Learn Cybern 2015. http://dx.doi.org/10.1007/s13042-015-0431-9.
[26] Mukherjee V, Ghoshal SPP. Intelligent particle swarm optimized fuzzy PID controller for AVR system. Electr Power Syst Res 2007;77:1689–98. http://dx.doi.org/10.1016/j.epsr.2006.12.004.
[27] Jahedi G, Ardehali MM. Genetic algorithm-based fuzzy-PID control methodologies for enhancement of energy efficiency of a dynamic energy system. Energy Convers Manag 2011;52:725–32. http://dx.doi.org/10.1016/j.enconman.2010.07.051.
[28] Shabib G. Implementation of a discrete fuzzy PID excitation controller for power system damping. Ain Shams Eng J 2012;3:123–31. http://dx.doi.org/10.1016/j.asej.2011.12.001.
[29] M. Estakhroueih Rezaei,, Gharaveisi A. Optimal iterative learning control design for generator voltage regulation system. Turkish J Electr Eng Comput Sci 2013;1909–19. http://dx.doi.org/10.3906/elk-1203-19.
[30] Sikander A, Thakur P, Bansal RC, Rajasekar S. A novel technique to design cuckoo search based FOPID controller for AVR in power systems. Comput Electr Eng 2017;1–14. http://dx.doi.org/10.1016/j.compeleceng.2017.07.005.
[31] Priyambada S, Sahu BK, Mohanty PK. Fuzzy-PID controller optimized TLBO approach on automatic voltage regulator. In: 2015 Int conf energy, power environ towar sustain growth. 2016, http://dx.doi.org/10.1109/EPETSG.2015.7510115.
[32] Panda MK, Pillai GN, Kumar V. Design of an interval type-2 fuzzy logic controller for automatic voltage regulator system. Electr Power Compon Syst 2011;40:219–35. http://dx.doi.org/10.1080/15325008.2011.629336.
[33] Sahib MA. A novel optimal PID plus second order derivative controller for AVR system. Eng Sci Technol Int J 2015;18:194–206. http://dx.doi.org/10.1016/j.jestch.2014.11.006.
[34] Prasad LB, Gupta HO, Tyagi B. Application of policy iteration technique based adaptive optimal control design for automatic voltage regulator of power system. Int J Electr Power Energy Syst 2014;63:940–9. http://dx.doi.org/10.1016/j.ijepes.2014.06.057.
[35] Gupta M, Srivastava S, Gupta JRP. A novel controller for model with combined LFC and AVR loops of single area power system. J Inst Eng Ser B 2016;97:21–9. http://dx.doi.org/10.1007/s40031-014-0159-z.
[36] Fan Lingling. Review of robust feedback control applications in power systems. In: 2009 IEEE/PES Power Systems Conference and Exposition. IEEE; 2009, p. 1–7.
[37] Bevrani H. Robust load frequency controller in a deregulated environment: A μ-synthesis Approach. In: Proc. 1999 IEEE, international conf. control appl.; 1999, p. 616–21.
[38] Haddadi A, Boulet B, Yazdani A, Joos G. A μ-based approach to small-signal stability analysis of an interconnected distributed energy resource unit and load. IEEE Trans Power Deliv 2015;30:1715–26. http://dx.doi.org/10.1109/TPWRD.2014.2380788.
[39] Han Y, Jain A, Young P, Zimmerle D. Robust control of microgrid frequency with attached storage system. In: Proc. IEEE conf. decis. control. 2013, p. 3043–8. http://dx.doi.org/10.1109/CDC.2013.6760346.
[40] Han Y, Young PM, Jain A, Zimmerle D. Robust control for microgrid frequency deviation reduction with attached storage system. IEEE Trans Smart Grid 2015;6:557–65. http://dx.doi.org/10.1109/TSG.2014.2320984.
[41] Shayeghi H, Ghasemi A, Shokri G. Vepso based PID with low pass filter for LFC design. Int J Tech Phys Probl Eng 2013;5:66–73.
[42] Zhao Q, Jiang J. Robust controller design for generator exitation systems. IEEE Trans Energy Convers 1995;10:201–9.
[43] Senjyu T, Morishima Y, Yamashita T, Uezato K, Fujita H. Decentralized H∞ excitation controller achieving damping of power system oscillations and terminal voltage control for multi-machine power. In: Transm. distrib. conf. exhib. 2002 Asia Pacific. IEEE/PES. IEEE; 2002, p. 174–9. http://dx.doi.org/10.1109/TDC.2002.1178279.

[44] Gu D-W, Petkov PH, Konstantinov M. Robust control design with MATLAB®. London: Springer-Verlag; 2005, http://dx.doi.org/10.1007/b135806.
[45] Chen S, Malik OP. H∞ optimisation-based power system stabiliser. IEE Proc Gener Transm Distrib 1995;142:179. http://dx.doi.org/10.1049/ip-gtd:19951711.
[46] F.K. A, Yorino N, Sasaki H. Design of H∞-PSS using numerator-denominator uncertainty representation. IEEE Trans Energy Convers 1997;12:45–50.
[47] Chen S, Malik M. Power system stabilizer design using μ-synthesis. IEEE Trans Energy Convers 1995;10:175–81. http://dx.doi.org/10.1109/60.372584.
[48] Saadat H. Power system analysis. 3rd ed. PSA Publishing; 2010.
[49] Lv C, Hu X, Sangiovanni-Vincentelli A, Li Y, Martinez CM, Cao D. Driving-style-based codesign optimization of an automated electric vehicle: A cyber-physical system approach. IEEE Trans Ind Electron 2019;66:2965–75. http://dx.doi.org/10.1109/TIE.2018.2850031.
[50] Lv C, Liu Y, Hu X, Guo H, Cao D, Wang FY. Simultaneous observation of hybrid states for cyber-physical systems: A case study of electric vehicle powertrain. IEEE Trans Cybern 2018;48:2357–67. http://dx.doi.org/10.1109/TCYB.2017.2738003.
[51] Lv C, Xing Y, Lu C, Liu Y, Guo H, Gao H, et al. Hybrid-learning-based classification and quantitative inference of driver braking intensity of an electrified vehicle. IEEE Trans Veh Technol 2018;67:5718–29. http://dx.doi.org/10.1109/TVT.2018.2808359.
[52] Péter G, Max G, Kiss B. Implementation of a robust electric brake actuator design based on H-infinity control theory. Period Polytech Transp Eng 2018;1–8. http://dx.doi.org/10.3311/pptr.12104.
[53] Lu Q, Sorniotti A, Gruber P, Theunissen J, De Smet J. H∞ loop shaping for the torque-vectoring control of electric vehicles: Theoretical design and experimental assessment. Mechatronics 2016;35:32–43. http://dx.doi.org/10.1016/j.mechatronics.2015.12.005.
[54] Nwesaty W, Bratcu AI, Sename O. Power sources coordination through multivariable LPV / Hinf control with application to multi-source electric vehicles. IET Control Theory Appl 2016;10:2049–59. http://dx.doi.org/10.1049/iet-cta.2015.1163, To cite this version : HAL Id : hal-01342899 Power sources coordination through multivariable LP V / H ∞ control with application to mul.
[55] Shourangiz-Haghighi A, Haghnegahdar MA, Wang L, Mussetta M, Kolios A, Lander M. State of the art in the optimisation of wind turbine performance using CFD. Arch Comput Methods Eng 2019;1–19.
[56] Yang B, Yu T, Shu H, Zhu D, Zeng F, Sang Y, et al. Perturbation observer based fractional-order PID control of photovoltaics inverters for solar energy harvesting via Yin-Yang-Pair optimization. Energy Convers Manag 2018;171:170–87.
[57] Li X, Wang Y, Li N, Han M, Tang Y, Liu F. Optimal fractional order PID controller design for automatic voltage regulator system based on reference model using particle swarm optimization. Int J Mach Learn Cybern 2017;8:1595–605. http://dx.doi.org/10.1007/s13042-016-0530-2.
[58] Doyle J. Analysis of feedback systems with structured uncertainties. IEE Proc D Control Theory Appl 1982;129:242–50. http://dx.doi.org/10.1049/ip-d.1982.0053.
[59] Zhou K, Doyle JC, Glover K. Robust and optimal control, vol. 40. Prentice Hall; 1996, http://dx.doi.org/10.1016/0967-0661(96)83721-X.
[60] Shao X, Liu J, Wang H. Robust back-stepping output feedback trajectory tracking for quadrotors via extended state observer and sigmoid tracking differentiator. Mech Syst Signal Process 2018;104:631–47. http://dx.doi.org/10.1016/j.ymssp.2017.11.034.
[61] Shao X, Wang L, Li J, Liu J. High-order ESO based output feedback dynamic surface control for quadrotors under position constraints and uncertainties. Aerosp Sci Technol 2019;89:288–98. http://dx.doi.org/10.1016/j.ast.2019.04.003.
[62] Shao X, Liu J, Cao H, Shen C, Wang H. Robust dynamic surface trajectory tracking control for a quadrotor UAV via extended state observer. Internat J Robust Nonlinear Control 2018;28:2700–19. http://dx.doi.org/10.1002/rnc.4044.
[63] Tepljakov A, Petlenkov E, Belikov J. FOMCON: a MATLAB toolbox for fractional-order system identification and control. Int J Microelectron Comput Sci 2011;2:51–62.
[64] Castillo O, Melin P, Castro JR. Computational intelligence software for interval type-2 fuzzy logic. Comput Appl Eng Educ 2013;21:737–47. http://dx.doi.org/10.1002/cae.20522.
[65] Model hydraulic turbine and proportional–integral–derivative (PID) governor system - Simulink. 2019, https://nl.mathworks.com/help/physmod/sps/examples/synchronous-machine.html. [Accessed 9 March 2019].
[66] Group IW. Hydraulic turbine and turbine control models for system dynamic studies. IEEE Trans Power Syst 1992;7:167–79.
[67] Implement generic power system stabilizer for synchronous machine - Simulink - MathWorks Benelux. 2019, https://nl.mathworks.com/help/physmod/sps/powersys/ref/genericpowersystemstabilizer.html?searchHighlight=GenericPowerSystemStabilizer&s_tid=doc_srchtitle. [Accessed 9 March 2019].
[68] Performance of three PSS for interarea oscillations - MATLAB & Simulink - MathWorks Benelux. 2019, https://nl.mathworks.com/help/physmod/sps/examples/performance-of-three-pss-for-interarea-oscillations.html. [Accessed 10 March 2019].
[69] Klein M, Rogers GJ, Moorty S, Kundur P. Analytical investigation of factors influencing power system stabilizers performance. IEEE Trans Energy Convers 1992;7:382–90. http://dx.doi.org/10.1109/60.148556.